Striations and hollow channels in rounded beryl crystals

Gioacchino Tempesta[*], Eugenio Scandale and Giovanna Agrosì

Dipartimento Geomineralogico, Università di Bari, Italy
[*]Corresponding author: *tempesta@geomin.uniba.it*

Abstract

Structural defects in natural colourless beryl crystals from Minas Gerais (Brazil) were studied using X-ray Diffraction Topography (XRDT). The samples are characterised by a strongly rounded morphology and by the presence of hollow channels parallel to the c-axis, some of them visible to the naked eye and partially filled with kaolinite. The analysis of structural defects as dislocations, growth bands, solid inclusions and precipitates has been essential for the reconstruction of growth history in this study. The formation of hollow channels was attributed to the corrosion and post-genetic alteration of strongly deformed areas surrounding branches of dislocations parallel to the c-axis. The final rounded morphologies and the striations may have been attained either as the results of a parallel growth of some individuals or as the result of a variation of the growth rates in the final stages of growth. Due to the occurrence of kaolinite, post-genetic corrosion has been speculated. However, this process appears to have contributed solely to the hollow channel formation and not to the rounded morphology evident in these samples.

Key words: X-ray topography; beryl; channels; morphology and striations.

Introduction

The morphology of natural crystals strongly depends not only on the crystal structure but also on the environmental growth conditions. Morphology may be also regulated by impurity absorption and dissolution-corrosion and alteration (weathering, erosion, transportation and burial). Characterizing growth and post-growth effects can lead to a better understanding of growth conditions (P, T, X) as morphological features could be related to specific growth conditions (e.g.: striations on prism faces which are vertical in tourmaline and horizontal in quartz).

Rounded morphologies, pipe-like channels and irregular voids are fairly common in a number of minerals in different growth environments and are often thought to have a post-growth origin. Yet their origins are under discussion, with different possible mechanisms being hypothesized. The exact mechanism in operation may depend not only on the crystal's structure but also on the conditions present during and after growth. And

yet, even if rounded morphologies do depend on the last stages of dissolution-corrosion (weathering, erosion, transportation and burial), crystals that grow at high supersaturations (Argiolas and Baumer, 1978; Sunagawa, 1984) may also be rounded.

In general, channels are to be expected with screw dislocations of large Burgers vectors (Frank, 1951; Baronnet, 1972; Dudley et al., 1999) or with bunching of hundreds of parallel dislocations and subsequent selective corrosion of dislocation-core material (Scandale and Zarka, 1982). Channels are also related to hollow elongated cavities due to inclusion absorption (Kawasaki et al., 2003; Minkoff, 1965). Voids may result not only from the bunching of channels (Scandale et al., 1993) but also from branched crystal growth (Minkoff and Nixon, 1966) and from spherulitic growth (Morse and Donnay, 1936) or from negative crystals.

Striations and thin parallel grooves on some crystal faces of minerals, synthetic crystals and kidney stones, are often attributed to the convergence or juxtaposition of two or more small crystal faces (Smolsky et al., 1999; Tolansky, 1945) belonging to the same or different morphological forms. Lamellar twinning, hundreds of twins repeated in a single specimen, is also considered a common cause of striations (Akizuki et al., 2001) as well as corrosion effects (Akizuki et al., 2001).

The reconstruction of growth history on minerals with X-ray Diffraction Topography-XRDT (Authier and Zarka, 1994; Scandale, 1996) can aid in answering some general questions. Recently, the growth history reconstruction of tourmaline crystals, occurring in pegmatite pockets on Elba Island (Italy), strongly suggests a relationship between tourmaline striations and the transition from pegmatitic to hydrothermal growth stages (Agrosì et al., 2006). In particular, two main growth stages - the first one pegmatitic and the second one hydrothermal - have been identified

and the observed striations may be connected with a near parallel intergrowth of small blocks, elongated along the c-axis, which developed in the final hydrothermal growth stage.

These results prompted us to investigate the occurrence of striations on beryl crystals in order to determine if there are general links between the development of striations, a channel's origin and the transition from magmatic to hydrothermal pegmatite growth. The results shown here indicate that the origin of both vertical striations and channels cannot be simply attributed to a single cause and that XRDT is a basic scientific tool that can contribute to our understanding of the mechanisms which are responsible for the observed growth features.

Methods and Techniques

Geological Background

The samples used in the study originate from the Coronel Murta district (Minas Gerais), a part of the Oriental Pegmatitic Province of Brazil. The pegmatites of this province are of a wide typological and geochemical variety (Sá, 1977). These pegmatites of Brasiliano-cycle have been dated 525 Ma (Siga Jr., 1986) and intrude into biotite - andalusite kyanite and staurolite bearing schist (Costa, 1987) that correspond to a metamorphosed flysch of the Eocambrian Salinas Formation. They are associated with two-micas and tourmaline granites. These pegmatites are lithaniferous and the Li, Rb and Cs contents vary in each zone of each pegmatite body.

Samples

Natural beryl crystals from Minas Gerais (Brazil) were examined and found to share coarse rounded elongated prism morphology which presents vertical striations, on the prism faces, hollow channels and irregular voids parallel to the c-axis, in the inner zones, within which a white powder identified as kaolinite was observed.

The results presented here discuss three natural colourless beryl crystals labelled HB1, HB2 and HB3 which are representative of the other crystals studied. The samples are elongated, strongly rounded $\{10\bar{1}0\}$ and $\{11\bar{2}0\}$ prisms, terminating in a prominent $\{0001\}$ pinacoid. Beryl HB1 has a length of about 3.2 cm and a basal section of about 1.3 x 0.9 cm; beryl HB2 has a length of about 2.6 cm and a basal section of 0.8 x 0.9 cm; and beryl HB3 has a length of about 3.6 cm and a basal section of 0.6 x 0.7 cm. Beryl HB1 and HB2 were studied using X-ray Diffraction Topography (XRDT), Powder XRD, and Optical Microscopy, whereas HB3 was studied with Optical Microscopy and Powder XRD only.

To reconstruct the growth history, 9 basal slices labelled from bottom to top L1 to L9 were cut from HB1 (Figure 1) and 7 basal slices labelled from L1 to L7 were obtained from HB2 (Figure 2). Structural defects were investigated using XRDT on slice HB1-L8 and on slices HB2-L2, HB2-L4 and HB2-L6.

X-ray Diffraction Topography (XRDT)

XRDT is an imaging technique based on Bragg diffraction and can characterize extended defects in nearly perfect crystals (Lang, 1959). The size of the slices, up to several cm^2 in the cross-sectional basal area and up to a few millimetres in thickness, ensures that the structural defects observed are typical of the bulk samples. Mapping of structural defects represents the local variations of diffracted intensities and/or diffracted beam directions produced by the strain fields which are associated with extended defects and/or distortions in the single-crystal lattice. XRDT techniques yield spatial distribution and full characterization of the crystal defects in the
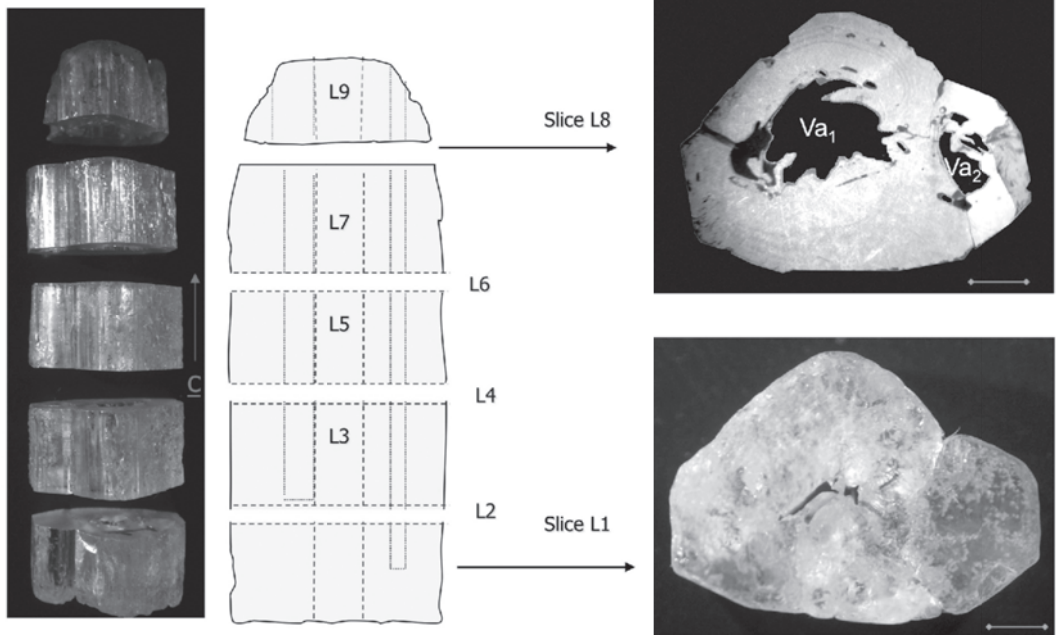

Figure 1. Optical pictures and reconstruction by sketch of the slices of HB1 hollow beryl crystal; L1 to L9 labels of the parts in witch the sample has been cut, Va1 and Va2 voids (bar scale = 2 mm).
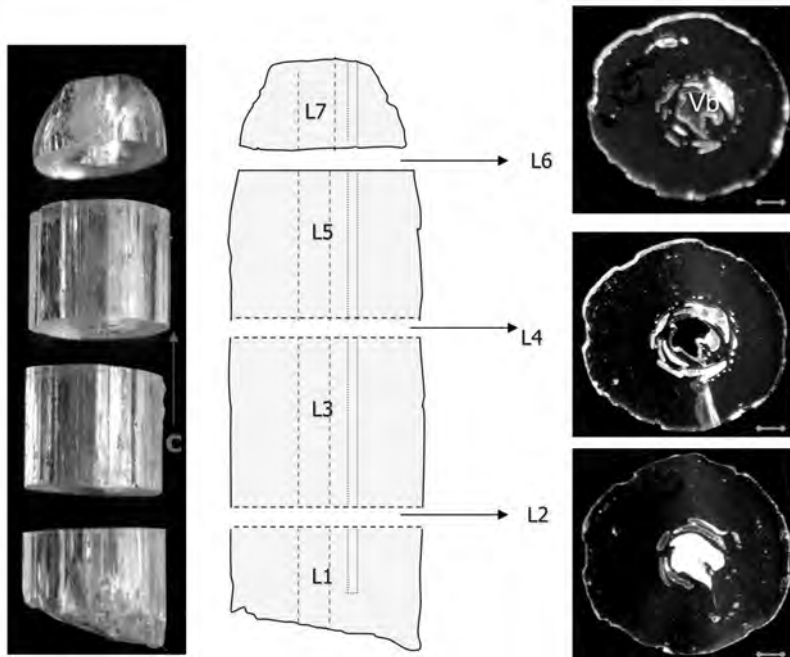
Figure 2. Optical pictures and reconstruction by sketch of the slices of HB2 hollow beryl crystal; L1 to L7 labels of the parts in witch the sample has been cut, Vb void (bar scale = 1mm).

whole sample volume. The technique used here is the Lang method with Laue geometry (Lang, 1959). The X-rays originated from a point source and were collimated by a vertical slit (aperture 150 μm) and a horizontal one (covering the whole sample). The collimated beam was directed at the crystal specimen, which was orientated to the Bragg angle. A regulating vertical slit, next to the sample, allowed the diffracted beam to be recorded on high resolution photographic plates and at the same time acted as a beam-stop for the transmitted beam. To study the whole sample, the crystal and the photographic plate were set on a platform equipped with a constant translation movement and scanned together through the X-ray beam. The traverse XRDTs shown here were carried out using a C.G.R. camera with monochromatic radiation (MoKα₁) and with a micro-focus X-ray tube. The beryl slices were about 1 mm thick, to satisfy the optimum diffraction condition $\mu t \approx 1$ (μ = linear absorption coefficient; t = crystal thickness) and to minimize X-ray absorption.

The slices were mechanically polished on both surfaces by SiC powders and diamond pastes down to 0.25 μm. Characterization of the structural defects was performed by applying the extinction criteria to their diffraction contrasts, according to kinematic and dynamic X-ray diffraction theories (Authier and Zarka, 1994).

X-ray Powder Diffraction

The white powders found in some channels of beryl HB1 and HB2 were prepared to be analysed by means of X-ray powder diffraction. The analyses were performed with an automated X'Pert Pro MPD X-ray Powder Diffractometer with a Bragg-Brentano geometry. The radiation was CuKα₁ monochromatized by a curved-crystal monochromator containing a graphite

crystal. The step scans were 0.02° as 2θ and the step time was 0.8 seconds while the angular range was 2θ = 5° - 75°. The spectrum analysis, performed with a specific software (X'Pert Graphics and Identify), identified the white powder as kaolinite $Al_2Si_2O_5(OH)_4$.

Results

Optical Observations

Optical Microscopy (OM) showed vertical striations and parallel grooves on the prism faces (Figures 1 and 2). Pyramidal etch patterns, with strongly [0001] elongated pseudo-hexagonal bases, were observed on the prism faces of both samples and are similar to those observed on beryl crystals from Elba Island (Italy) previously studied with XRDT (Scandale et al., 1990). No relations were found between the etch patterns and bulk structural defects.

Pipe-like hollow channels parallel to the c-axis with diameters ranging from about 1 to 500 microns are present in the inner zones and generally outcrop on the basal face, exhibiting various morphologies, from conic-cylindrical to sharp hexagonal, with edges parallel to the {10$\bar{1}$0} and {11$\bar{2}$0} prism faces (Figure 3). A few channels contain fluid inclusions and others are optically discontinuous. Similar optical observations had been made in other synthetic and natural crystals, beryl included (Scandale and Zarka, 1982; Agrosì et al., 2005).
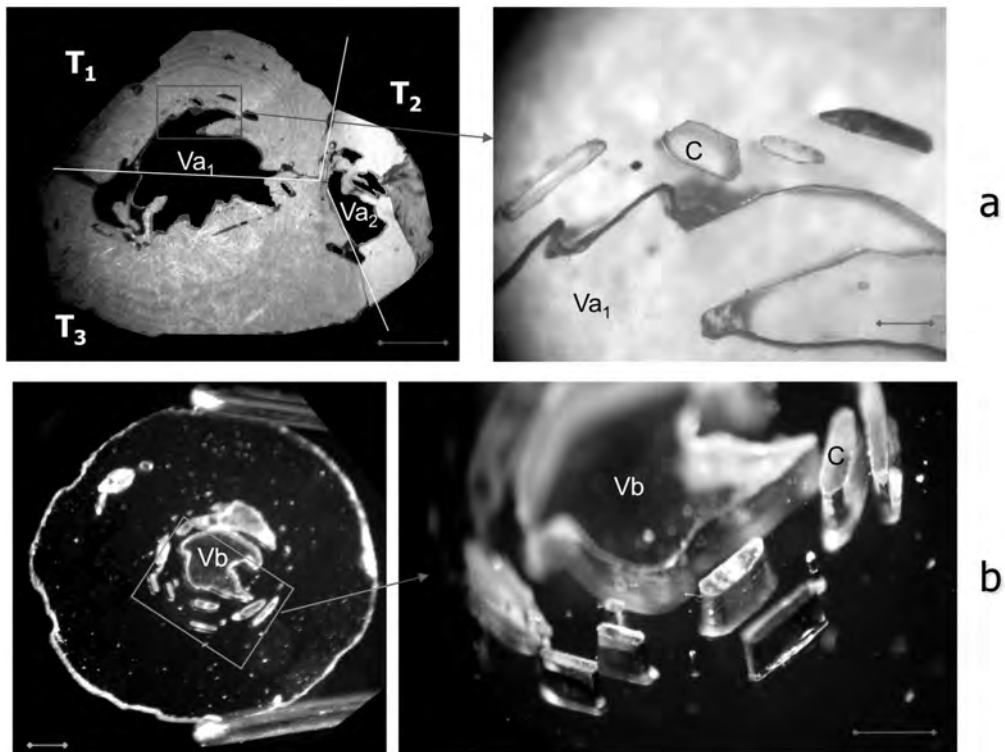
Large irregular voids, often penetrating

Figure 3. a) Optical image of the slice HB1-L8 and enlarged details of channels and voids (bar scale on the left = 2 mm; bar scale on right 0.2 mm); b) Optical image of the slice HB2-L6and enlarged details of channels and void (bar scale on the left = 1 mm; bar scale on right 0.5 mm).

through the entire sample, were observed in the central inner cores. Voids and the larger channels, visible to the naked eyes, are often filled with a white polycrystalline material that was found to be kaolinite. A closer observation confirmed that the channels and voids, crossing the sample, are filled with kaolinite, continuously from top to bottom in some cases and in others discontinuously in a dashed trail.

The large central irregular voids in both samples present different shapes in the different slices (Figures 1 and 2). In particular, it can be observed that void V_a in HB1 changes from top to bottom, splitting into smaller voids while its total empty area decreases. On the contrary, in HB2, void V_b retains the outline while its internal area increases slightly from top to bottom. The channels C of HB1 and HB2 are parallel and their shape matches the morphological faces. It could be observed that the different slices change dimensions and contours and that the channel abundance of HB2 is less than that of HB1.

Large uneven voids V and channels C can be noted in Figure 3. The larger voids V_{a1} and V_{a2} separate blocks T_1, T_2 and T_3 from each other, whereas the smaller ones are contained within the blocks. Most channels are localized in block T_1 where they can be divided into two groups. In fact, those close to the external rim have elongated hexagonal shapes with sides parallel to the morphological faces while the others, near the internal rim, have a mainly rounded elliptic shape with a long semi-major axis parallel to the crystal faces.

Observations under crossed polarisers revealed an anomalous wavy extinction originating from the channels in HB2 and from differently oriented crystal domains in HB1 (Figure 4).

X-ray Topographic Observations

XRDT images of all basal slices of the HB1 and HB2 samples were taken with the three $10\bar{1}0$ equivalent reflections. The diffraction contrasts observed with the equivalent reflections result quite similar in type and distribution and thus,
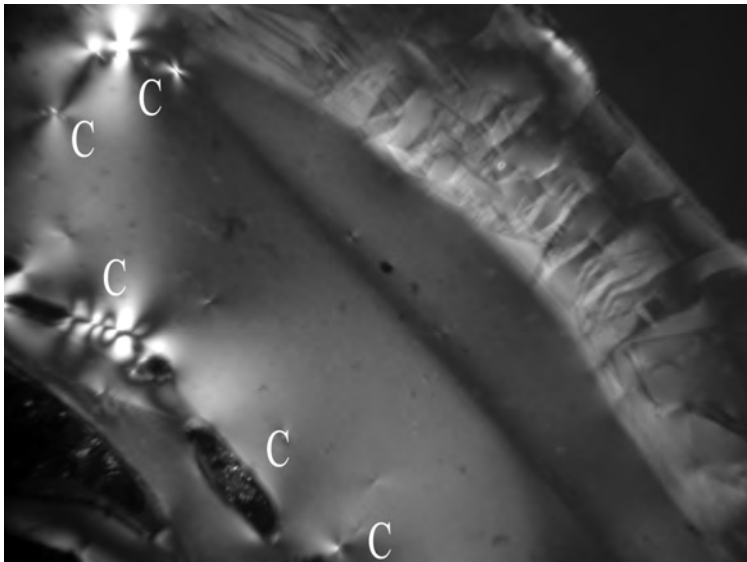

Figure 4. Optical image using crossed polarizes of a detail of the studied slice L6 of HB2 showing stress areas around channels.
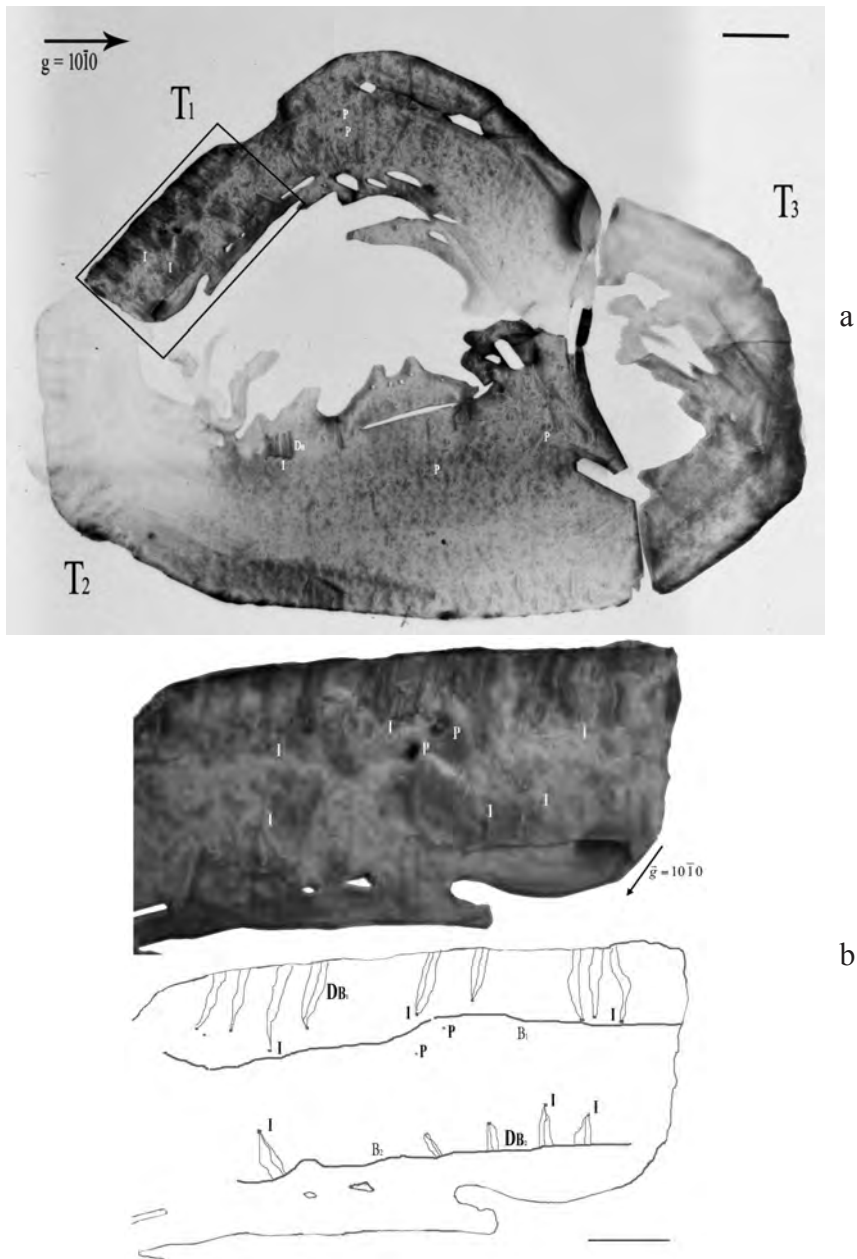
Figure 5. a) XRDT of HB1-L8 obtained combining three topographs, taken with the same diffraction vector **g** = 10$\bar{1}$0 from regions (T1, T2 and T3) slightly disoriented (bar scale = 1 mm); b) Enlarged detail of HB1-L8 topograph shown in Figure 5 coupled with a sketch of T1 representing dislocation bundles DB1 nucleated from inclusions adsorbed on boundary B1, and dislocation bundles DB2 ending on the growth stage boundary B2 (bar scale = 0.5 mm).
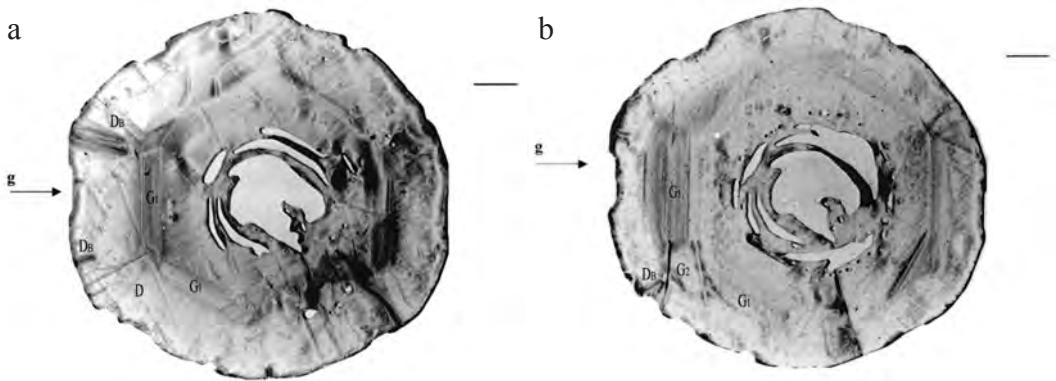
Figure 6. a) XRDT of HB2 L2 taken with the diffracting vector $\mathbf{g} = 10\bar{1}0$ (bar scale = 1 mm); b) XRDT of HB2 L4 taken with the diffracting vector $\mathbf{g} = 10\bar{1}0$; G1 and G2 = growth bands, DB = dislocation bundles (bar scale = 1 mm).

for the sake of brevity, only those taken with diffracting vector $\mathbf{g} = 10\bar{1}0$ will be shown and discussed here.

The topographs of HB1 (Figure 5) and those of HB2 (Figure 6 and 7) showed that the main structural defects of the studied crystals are precipitates (P), solid inclusions (I), dislocation bundles nucleated from solid inclusions (D_B), pipe-like channels (C), voids (V), and growth bands (G). The topographs demonstrated that even if the structural defects observed in the studied crystals are similar, the diffraction contrasts of each sample characterize and differentiate each other. For this reason it is necessary a separate illustration of the diffraction contrasts of the two samples was required.

HB1 sample

Figure 5 illustrates the composition of three topographs, T_1, T_2 and T_3, taken with the same diffracting vector $\mathbf{g} = 10\bar{1}0$ from slightly disoriented regions of the slice HB1-L8. The composition shows that the crystal is an aggregate of three independently diffracting blocks, coherently scattering, within which phase relationships hold. The complementary topographs were taken with the same diffracting vector $\mathbf{g}$ with

a rotation of a few seconds of arc about the Bragg angle $\theta_{10\bar{1}0}$.

In the blocks T_1 and T_3 basal dislocation bundle D_B (Figure 5b), with individual contrasts generally not resolved, nucleated from solid inclusions I, were observed in the late growth stages where the defect density increases. In the block T_1, dislocation bundles D_{B1} were nucleated from inclusions adsorbed on boundary B_1, whereas, dislocation bundles D_{B2} end on the growth stage boundary B_2 (Figure 5b). The D_{B1} dislocation lines point from B_1 towards the external rim whereas D_{B2} dislocation lines point to B_2, following two opposite growth directions, n_1 and n_2 respectively (Klapper, 1972; Graziani et al., 1981).

The inhomogeneous diffraction contrasts observed in the T_1 crystal region and bounded by B_1 and B_2, arise from local variations of diffracted intensities which were due to the strain fields associated to subgrain boundaries, as well as, from direction variation of the diffracted beams which were caused by misoriented grains. Therefore B_1 and B_2 boundaries are polygonal-lines made up of a large number of subgrain boundary sides of small dimensions.
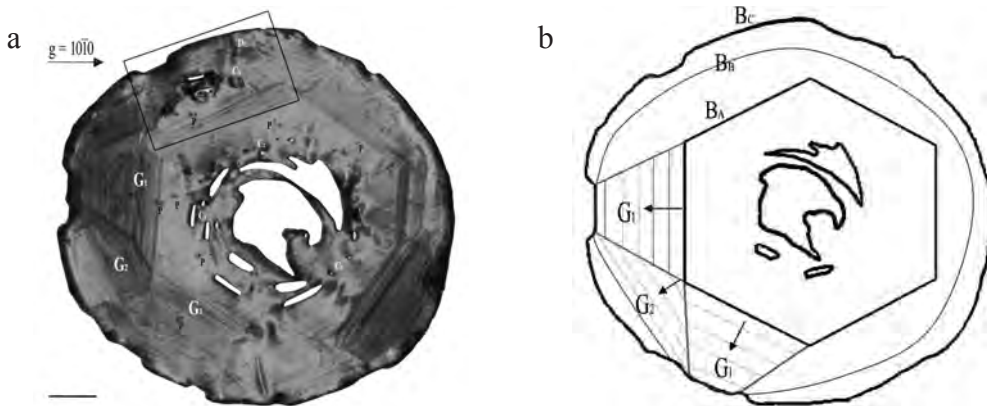
In T_1 and T_3, precipitates P were found

Figure 7. a) XRDT of HB2 L6 taken with the diffracting vector **g** = 10$\bar{1}$0; BA, BB and BC = growth stage boundaries, G1 and G2 = growth bands parallel to first-order and to second-order prism faces, P = precipitates, C = channels and DB = dislocation bundles (bar scale = 1 mm); b) sketch of the growth stage boundaries BA, BB and BC and of growth bands, G1 and G2.

together with their classical diffraction contrasts which consist of two circular parts connected together by a contrast-free plane normal to the operating diffracting vector **g** (Tanner, 1976).

HB2 sample

In Figures 6 and 7, topographs of the slices L2, L4 and L6 can be seen.

Three growth stage boundaries - B_A, B_B and B_C - and growth bands - G_1 and G_2 - parallel to {10$\bar{1}$0} first-order and {10$\bar{2}$0} second-order prism faces, respectively, can be observed (Figure 7a) and are outlined in Figure 7b. Notice the hexagonal contour, with sharp straight sides, of the growth stage boundary B_A and the strongly rounded one of B_B. The decreasing widths of the growth bands observed in the L6 topograph, clearly indicate an increased growth rate in the late growth stage of the first order prism faces. At the same time, the growth rates of the vicinal faces are reduced.

Rare and isolated dislocations D, nucleated at the boundaries B_A and B_B, and basal dislocation bundles D_B, nucleated at the boundary B_B could be observed. Their different dislocation line orientations indicate the normal growth in the

different growth sectors (Klapper, 1972).

Figure 8 illustrates different groups of dislocations D_B parallel to the basal plane which were nucleated from inclusions (I) absorbed during the last stages of growth. The dislocation lines of the group D_B appear to be convergent towards the crystal rim, whereas the other dislocations observed in the HB2 slices, due to their elastic repulsion, show a normal divergent fan configuration (Figure 6a). The peculiar feature of D_B can only be explained by speculating that they were generated from different inclusions at different depths in the slice and that the distances are such that their elastic field cannot interact. As seen Figure 8, the hexagonal contour of a crystalline region C_X always shows a characteristic topographical contrast of a bundle of dislocations parallel to the c-axis.

The diffraction contrasts of channels (C_2 and C_3 in Figure 7a) consist of two contributions. The first one corresponds with the black contrast due to the rim effects while the second is associated with the residual strain fields of a parallel dislocation bunching (Scandale and Zarka, 1982). Void and some of the high channel

contrasts (V_b and C_1 Figure 7a) depend solely on the rim effects.

The topographic contrasts of C_4 and C_5 (Figure 8) are to be expected with bunching of hundreds of parallel dislocations (Scandale and Zarka, 1982). Precipitates P, similar to those seen in HB1, can be observed mainly in the first growth stage (Figure 7) on occasion in the other ones.

Discussion and Conclusions

The present study aims at reconstructing the growth history of selected colourless pegmatitic beryl crystals, HB1 and HB2, from Minas Gerais (Brazil). Upon examination of the crystals, particularly slice L6 of HB2 and slice L8 of HB1, the following common morphological features were observed:

1) colourless and elongated parallel to the c-axis, with striation and a rounded morphology;

2) crossed by voids and channels parallel to the c-axis;

3) smaller channels show often an hexagonal outline with sides parallel to the prism faces;

4) some channels are filled with kaolinite $[Al_2Si_2O_5(OH)_4]$;

5) similar etch patterns are noted on the prism faces.

All these common morphological elements, in addition to the same geological occurrence, suggest that the HB1 and HB2 samples grew, were corroded and altered in very close chemical and physical conditions. Consequently, they should have a quite similar growth history.

The study of structural defects could demonstrate that this hypothesis is only partially true. Whereas it is likely that the samples grew, were corroded and altered in a similar way, the growth history reconstruction of HB1 and HB2 obtained by examination of the structural defects indicates that the main common features, i.e., the rounded morphologies and striations, may have been attained through two different growth mechanisms.

Sample HB1 consists of an aggregation of individual elongated crystals that are rotated slightly to each other about the c-axis. The parallel intergrowth of those crystals induce the
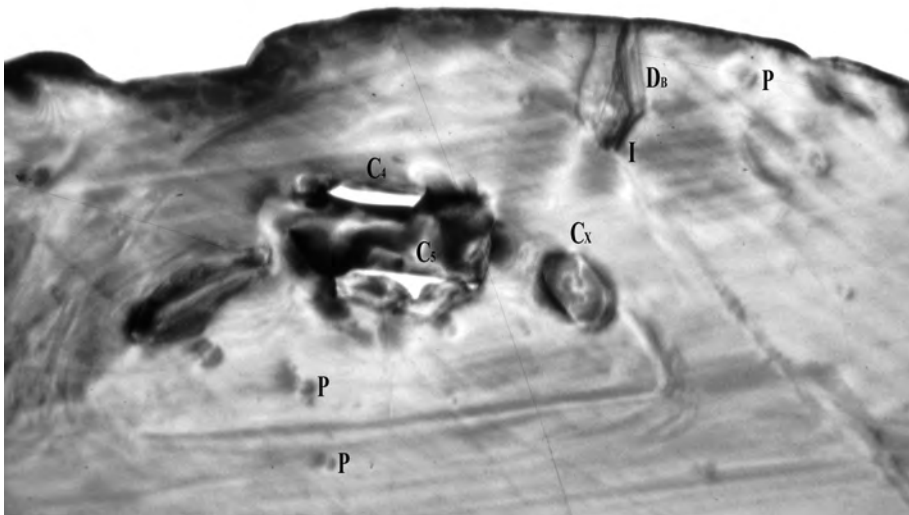

Figure 8. Enlarged detail of HB2 L6 topograph shown in Figure 7a (bar scale = 0.35 mm).

formation of cavities and voids in the inner part and striations on the morphological faces.

Due to the fact that voids and cavities are bounded by morphological faces of different mineral individuals, it can be observed that the growth occurs in opposite directions. As an example, Figure 5b illustrates bundles of D_B dislocations perpendicular to the outer rim B_1 vand to the growth stage boundary B_2, that point in opposite directions starting from solid inclusions I.

Post-genetic selective dissolution, driven by the deformation fields of dislocation bundles (Scandale and Zarka, 1982) may have contributed also to the formation of channels and irregular voids in the inner parts of the individual grains and not to the rounded morphology of the sample. The final alteration resulted in the formation of kaolinite inside the larger channels and irregular voids.

The observation and the analysis of the defects of the crystal HB1, shows that the defects are identical to those revealed in HB2 but that their distribution could point to a different evolution.

In the case of beryl HB2, the final morphology is mainly due to an abrupt increase of the growth rates of the first-order prism faces $\{10\bar{1}0\}$ with respect to second-order prism $\{10\bar{2}0\}$ (Figure 7). Hence, the rounded morphology may not be the result of a strong corrosion process but, instead, the result of a dramatic variation of the growth velocities of the crystal faces as seen in the diffraction images.

The HB2 topographs provide clear evidence of well-defined growth marks as observed in all the topographs. In fact, it is possible to draw various growth boundaries in the crystal, which represent the complete evolution, as it follows from the schematic illustration in Figure 7b.

Upon observation of the growth boundaries, two main boundaries could be identified: B_A and B_B (Figure 7b) which are connected to variations in growth conditions. The transition from the sharp hexagonal boundaries B_A to the rounded one B_B is related to asymmetrical variations of the growth velocities of the $\{10\bar{1}0\}$ and $\{10\bar{2}0\}$ growth sectors. From this we can draw the unequivocal conclusion that the early crystal shape was a hexagonal prism that over time became strongly rounded off. This most likely is not due to a secondary corrosion, as a first macroscopic observation of the striations might indicate, but because of (P, T, X).
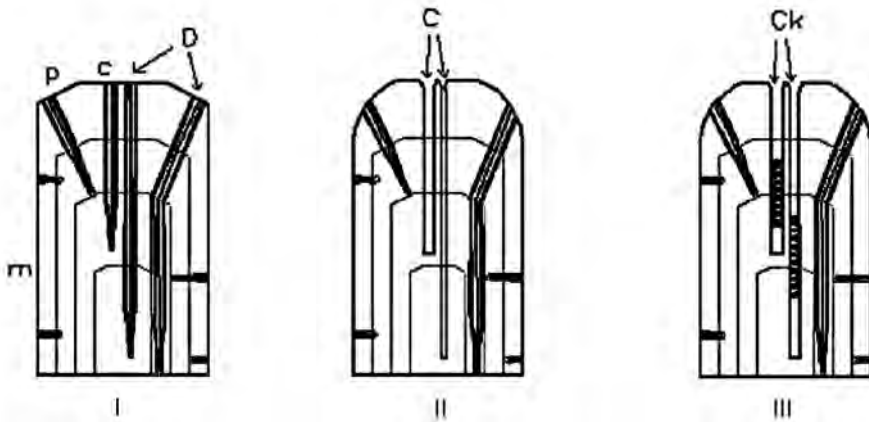

Figure 9. The schematic drawings of channels evolution; m = sectors $\{10\bar{1}0\}$; p = sectors $\{10\bar{1}1\}$; c = sectors $\{0001\}$; C = channels; D = dislocations; Ck = channels with kaolinite. Three stages are represented: I) growth, II) corrosion and III) corrosion and alterations.

X-ray topographs have been invaluable in finding the origin of channels. In fact, the topographic contrasts C_X (Figure 8) were able to localize the crystal region, where corrosion preferentially occured, due to the high strain concentration produced by the bundle of parallel dislocations (Scandale & Zarka, 1982).

Figure 9 is a schematic illustration describing in general terms the formation of the channels in HB1 and HB2. Three stages are represented: I) growth, II) corrosion, III) corrosion and alterations. Hence, the deformation fields, associated to the dislocation bundles normal to (0001), may have determined the favourable conditions for a preferential etching that produced the observed channels. However, the same mechanism does not appear to have operated on the dislocation bundles working on the sectors m $\{10\bar{1}0\}$ and p $\{11\bar{2}0\}$. There is in fact (Sangwal, 1987) an anisotropy in the macroscopic dissolutions rates; therefore on some faces the process is so slow to be considered negligible. Moreover, in agreement with the kinematic theory, anisotropy was the same when considering growth, and the nucleation rate and dissolution rate are proportional among them. In conclusion, it can be stated that the channels' origin is due to a post-genetic corrosion.

It seems therefore that the X-ray topography method is central in the reconstruction of the growth history of natural crystals. This technique can give answers to mineralogical problems originating from the fact that the conditions of crystal growth are still not fully understood. All the common features analysed indicate that HB1 and HB2 originated from a geological environment with similar chemical and physical conditions. However, the analysis of the structural defects using XRDT confirmed that two kinds of growth mechanisms occurred: a parallel growth for the HB1 sample; and a single crystal growth with a different growth rate on the faces of the first order and second order prism for the HB2 sample.

References

Agrosì G., Fregola R.A., Monno A., Scandale E. and Tempesta G. (2005) - XRDT Study of Structural Defects of 6H-SiC Crystals. *Materials Science Forum*, 483-485, 311-314.

Agrosì G., Bosi F., Lucchesi S., Melchiorre G. and Scandale E. (2006) - Mn-tourmaline crystals from island of Elba (Italy): Growth history and growth marks. *American Mineralogist,* 91, 944-952.

Akizuki M., Kuribayshi T., Nagase T. and Kitakaze A. (2001) - Triclinic Liddicoatite and Elbaite in Growth Sectors of Tormaline from Madagascar. *American Mineralogist*, 86, 364-369.

Appleman D.E. and Evans H.T. Jr. (1973) - Indexing and least-squares refinement of powder diffraction data. National Tech. Information Service, U.S. Department of Commerce, Springfield, Virginia, Doc. PB-216, 188.

Argiolas R. and Baumer A. (1978) - Synthése de chlorapatite par voie hydrothermale; étude de l'influence de la sursaturation sur l'évolution des faciés des cristaux. *Canadian Mineralogist*, 16, 285-290.

Authier A. and Zarka A. (1994) - X-ray topographic study of the real structure of minerals. In A.S. Marfunin Ed., Composition, Structure and Properties of Mineral Matter, Springer-Verlag, Berlin, 221-233.

Azaroff L.V., Kaplow R., Kato N., Weiss R.I., Wilson A.J.C., Young, R.A. (1974) - X-ray diffraction. Mc Graw Hill, New York.

Baronnet A. (1972) - Growth mechanisms and polytypism in synthetic hydroxyl-bearing phlogopite. *American Mineralogist*, 57, 1271-1293.

Costa A.G. (1987) - Petrologie und geochemische Untersuchungen des Gneis-Migmatite-Gebiets von Itinga, Jequitinhonha-Tal, Nordoestliches Minas Gerais, Brasilien. West Germany. (Dr. Thesis, TU-Clausthal).

Dudley M., Huang H.R. and Huang W. (1999) - Assessment of orientation and extinction contrast contributions to direct dislocation image. *Journal of Physics D*: Applied Physics, 32, A139-A144.

Frank F.C. (1951) - Capillary equilibria of dislocated crystals. *Acta Crystallographica*, 4, 497- 501.

Graziani G., Lucchesi S. and Scandale E. (1990) - General and Specific Growth Marks in Pegmatite Beryls. *Physics and Chemistry of Minerals*, 17, 379-384.

Graziani G., Scandale E. and Zarka A. (1981) - Growth of Beryl Single Crystal – History of development and genetic medium. *Journal of Applied Crystallography*, 14, 241-246.

Kawasaki M., Onuma K. and Sunagawa I. (2003) - Morphological instabilities during growth of rough interface: AFM observations of cobbles on the (0001) face of synthetic quartz crystals. *Journal of Crystal Growth*, 258, 188-196.

Klapper H. (1972) - Elastische Energie und Vorzugsrichtungen geradliniger. Versetzungen in aus der Losung gewachsenen organischen Kristallen. *Physica Status Solidi A*, 14, 99-106.

Lang A.R. (1959) - The projection topograph: a new method in X-ray diffraction microradiography. *Acta Crystallographica*, 12, 249-250.

Minkoff I. (1965) - Hole Formation in Crystal Growth by Surface Adsorption of an Impurity. *Philosophical Magazine*, 12, 1083-1086.

Minkoff I. and Nixon W.C. (1966) - Scanning Electron Microscopy of Graphite Growth in Iron and Nickel Alloys. *Journal of Applied Physics*, 37, 4848-4855.

Morse H.W. and Donnay D.H. (1936) - Optics and structure of three-dimensional spherulites. *American Mineralogist*, 21, 391-426.

Sá J.H. de (1977) - Pegmatitos litiniferos da região de Ilinga-Araçuaí. Ph. D. thesis, USP, São Paulo, Brasil.

Sangwal K. (1987) - Etching of Crystals: Theory, Experiment and Application. Defects in Solids, Amsterdam, Oxford, New York, Tokyo: North Holland, 15, 497.

Scandale E. and Lucchesi S. (2000) - Growth and sector zoning in a beryl crystal. *European Journal of Mineralogy*, 12, 357-366.

Scandale E. (1996) - Growth and Sector zonings. In E. Scandale and A. Baronnet, Eds., Crystal Growth in Earth Sciences, EDISU, Torino, 176-194.

Scandale E., Lucchesi S. and Graziani G. (1993) - Improvements on the growth history reconstruction of a beryl crystal by growth marks. *Neues Jahrbuch für Mineralogie Monatshefte,* 4, 172-184.

Scandale E., Lucchesi S. and Graziani G. (1990) - Growth defects and growth marks in pegmatite beryls. *European Journal of Mineralogy*, 2, 305-311.

Scandale E. and Zarka A. (1982) - Sur l'origine des canaux dans les cristaux. *Journal of Applied Crystallography*, 15, 417-422.

Scandale E., Scordari F. and Zarka A. (1979a) - Etude des défauts dans des monocristaux naturels de béryl. I. Observations des dislocations. J*ournal of Applied Crystallography*, 12, 70-77.

Scandale E., Scordari F. and Zarka A. (1979b) - Etude des défauts dans des monocristaux naturels de béryl. II, Etude de croissance. *Journal of Applied Crystallography*, 12, 78-83.

Siga Jr. O. (1986) - A evolução geocronológica da porão nordeste de Minas Gerais, com base em interpretações geocronológicas. Inst. Geociências, Universidade de São Paulo, São Paulo, Brazil, MSc thesis.

Smolsky I.L., Voloshin A.E., Zaitseva N.P., Rudneva E.B. and Klapper H. (1999) - X-ray topographic study of striation formation in layer growth of crystals from solutions. X-ray Topography and Crystal Characterization, Philosophical Transactions of the Royal Society of London, A 357, 2631-2649.

Sunagawa I. (1984) - Growth of crystals in nature. Materials science of the earth's interior, I. Sunagawa. *Terra Scientific Publishing*, Tokyo, 61-103.

Tanner B.K. (1976) - X-ray Diffraction Topography. Pergamon Press, Oxford.

Tolansky S. (1945) - The Topography of Crystal Faces. I. The Topography of a (100) Face of a Left-Handed Quartz Crystal. *Proceedings of the Royal Society of London*, A 184, 41-51.